A Fast Numerical Procedure for Steady Capillary Flow in Open Channels

J. Klatte[1], D. Haake[1], M. M. Weislogel[2], M. Dreyer[1]

[1]Center of Applied Space Technology and Microgravity,
University of Bremen, Bremen, 28359

[2]Department of Mechanical Engineering,
Portland State University, Portland, OR 97207

Abstract

The *Surface Evolver* (*SE*) algorithm is a valued numerical tool for computations of complex equilibrium interfacial phenomena. In this work an iterative procedure is implemented such that *SE* can be employed to predict steady state flows along capillary channels of arbitrary cross section. As a demonstration, a one-dimensional stream filament flow model is solved that approximates the pressure changes inside the channel. Despite its simplicity, the precision, stability, and speed of the method affirms it as an efficient and unique design tool for a variety of capillary flow problems. The procedure is ideally suited for slender column flows such as open wedge channel flows, several of which are validated herein via parabolic flight and drop tower experiments.

1   Introduction

Surface tension dominated flows along capillary channels are of significant practical interest, spanning microfluidic to macrofluidic phenomena from Lab-On-Chip technologies to microgravity fuels management aboard spacecraft. Despite continued advancements in computational methods and hardware, 3-d numerical Navier-Stokes solvers with interface tracking or interface interpolation methods continue to require a significant computational effort with long solution times limiting large parametric spaces to be studied thoroughly and efficiently. The method pursued herein presents a fast numerical tool for design and parametric studies of capillary flows in open channels.

For surface tension dominated problems, K. Brakke's [1] *Surface Evolver* (*SE*) algorithm is found to be a fast and useful tool to compute precise information about liquid position and interfacial area for steady state (i.e. 'equilibrium') problems. The algorithm solves for the minimum of the integrated user-defined energy for an arbitrary geometry subject to numerous user-defined constraints. Further applications, examples, and technical details can be found in the *SE* user manual [2]. Example applications, that implement user-defined energies can also be cited [3].

It is of practical interest to expand *SE*'s steady state capabilities by adding friction losses as well as convective pressure changes for constant flow rate problems in capillary channels. The aim of this article is to describe the present implementation of a 'dynamic' pressure model within *SE* and to identify its limits of applicability. Similarities in terms of grid management and iteration procedure exist to the more expensive and time-dependent Stokes solvers [4]. Exact analytic approaches for free surface flows in groove and wedge geometries exist [5, 6], but are limited herein to the viscous-dominated regime.

The proposed numerical procedure is demonstrated for liquid flows inside wedge and rectangular groove open capillary channels, where analytical and experimental data are available for comparison. As will be seen, interface profiles, flow rates, and flow rate limits compare well with the experimental data.

2   Model

A laminar, isothermal, incompressible, and Newtonian liquid flow through an open wedge-shaped channel is sketched in fig. 1. A passive overlying gas is assumed such that stresses at the interface may be neglected. The liquid-gas interface is represented with a moving finite element grid, and precise contact angle or pinning conditions can be defined at the interface boundaries. The liquid pressure $p(x)$ is approximated using the 1-d stream filament theory along the x-axis,
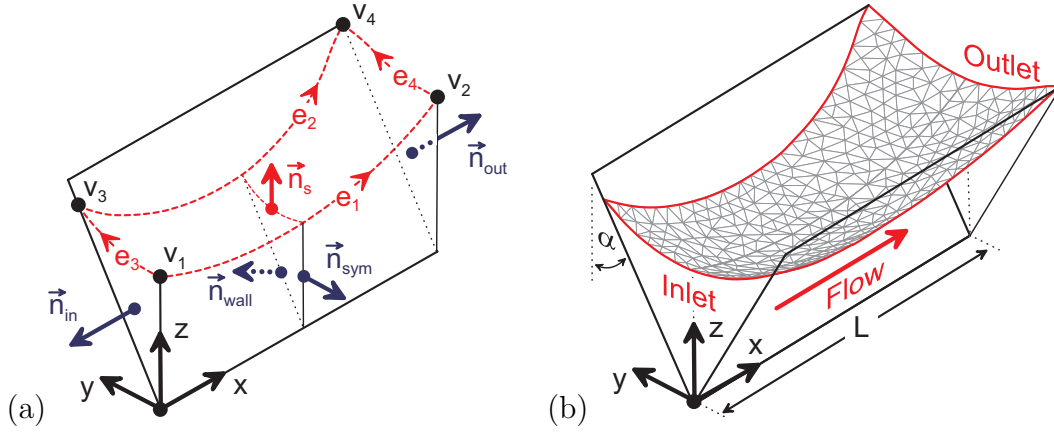
Figure 1: Notation for liquid flow in an open capillary wedge. The fluid flows from the inlet to the outlet area with a constant flow rate Q. (a) The initial sketch of SE with the boundary normals of the fluid volume V. The symmetry plane reduces computational time. (b) Graphical output of the interface between moving liquid in the corner and surrounding gas phase.

where

$$\frac{\rho}{2}\frac{Q^2}{A^2(x)} + p(x) + p_f(x) = C. \tag{1}$$

Employing a mass balance, the convective term with density ρ appears in eq. (1) as a function of the constant flow rate Q and cross-sectional area A. Constant pressure throughout each cross-section is assumed. The constant C is defined by the pressure difference to the overlying gas phase, but is insignificant if the liquid volume of the system is constant. The additional friction factor p_f,

$$p_f(x) = \frac{Q\eta}{2}\int_0^x \frac{K_\alpha(h(x'))}{D_h(x')^2 A(x')}dx', \tag{2}$$

with dynamic viscosity η and hydraulic diameter D_h, approximates the pressure loss along the flow. As one can see in table 1, numerical integrations of Poisson's equation are used to determine the pressure loss coefficient K_α. The friction model assumes a fully developed velocity profile at each cross-section and neglects transition losses [6, 7, 8]. As long as the fluid pressure $p(x)$ can be evaluated from the interface position, one is free to extend or modify the pressure model to suit.

In SE, the pressure $p(x)$ or any other quantity must be implemented as an energy integral over the liquid boundaries S, e.g. the surface tension σ is applied as a surface energy $E_\sigma = \iint_S \sigma dS$. With the definition

$$P(x) \equiv \int_0^x p(x')dx', \tag{3}$$

2
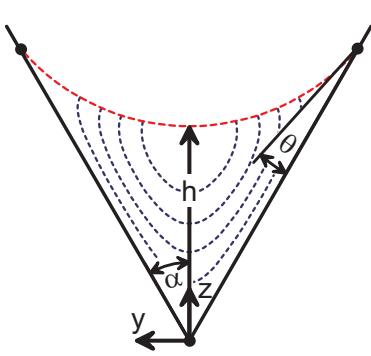
α	$\theta(h)$	K_{analy}	K_{num}	Diff.(%)
	10°	45.93	46.02	0.196
10°	40°	49.02	49.10	0.163
	70°	49.82	49.91	0.181
	10°	43.79	43.82	0.069
30°	30°	50.68	50.71	0.059
	50°	54.20	54.22	0.037
	10°	42.86	42.91	0.117
50°	20°	49.26	49.31	0.102
	30°	53.56	53.60	0.075

Table 1: A typical velocity contour and comparisons of analytical [9] and numerical [10] friction constants $K = \frac{2D_h{}^2}{\eta} \frac{A}{Q} \frac{\partial p}{\partial x}$ for fully developed laminar flow in an open capillary corner. Free slip and a constant curvature radius are assumed at the interface. The contact angle θ depends on the minimal interface height h. The good agreement validate the numerical tool, which can be used to calculate the pressure loss of arbitrary channels.

the divergence theorem applied to the energy E_p of the fluid pressure yields

$$E_p = \iiint_V p(x)dV = \iint_S \begin{pmatrix} P(x) \\ 0 \\ 0 \end{pmatrix} \cdot \mathbf{n}dS. \tag{4}$$

To simplify grid management and to save computational time, only the moving interface boundary S_s with normal $\mathbf{n_S}$ is modeled for the liquid volume V, as seen in fig. 1. The energy equation is thus an integral over the free surface S_s and its boundary edges e_{1-4}. Because all boundary normals except $\mathbf{n_S}$ are constant and $P(0) = 0$, eq. (4) yields

$$E_p = \iint_{S_s} \begin{pmatrix} P(x) \\ 0 \\ 0 \end{pmatrix} \cdot \mathbf{n_s}dS + P(L)S_{out}, \tag{5}$$

with the outlet area

$$S_{out} = \int_{e_4} \left(z - \frac{y}{\tan \alpha} \right) dy. \tag{6}$$

A general analytic expression with variable coefficients a_i is used to evaluate $P(x)$. First, the pressure $p(x)$ of eq. (1) is approximated by a 5th order polynomial

$$p(x) \approx a_0 + a_1 x + a_2 x^2 + a_3 x^3 + a_4 x^4 + a_5 x^5 \tag{7}$$

(note that higher order polynomials produce neglible improvements in accuracy).

3

Together, the pressure energy E_p yields

$$
\begin{aligned}
E_p \;\approx\; & \iint_{S_s} \left(a_0 x + \frac{a_1}{2} x^2 + ... + \frac{a_5}{6} x^6, 0, 0 \right) \cdot \mathbf{n_S} dS + \\
& + \left(a_0 L + \frac{a_1}{2} L^2 + ... + \frac{a_5}{6} L^6 \right) \int_{e_4} \left(z - \frac{y}{\tan \alpha} \right) dy.
\end{aligned} \tag{8}
$$

Thus far, dynamic channel flows are modeled as a pressure energy quantity within SE. However, the pressure field is coupled to the free surface shape and must be re-calculated during the computation using the following iterative procedure.

1. Calculate the flow pressure p_f using eqs. (1) and (2) at discrete points along the x-direction. The cross-section area $A(x)$ and the friction factor $K(\alpha, h(x))$ are evaluated from the interface shape.

2. Evaluate the new interpolation constants a_i of eq. (7) to update the pressure energy given by eq. (8).

3. Perform SE iterations to adapt the interface shape by minimizing the total energy of the system.

4. Repeat steps 1-3 until both the total energy and the coefficients a_i converge.

After terminating the iteration loop, the interfacial and flow pressures are balanced and a steady state solution for constant flow rate Q is obtained. Additional solution details are left to the appendix. The procedure requires several minutes on a standard desktop computer.

3   Applications and Validation

It is necessary to validate the numerical model and to show its generality for capillary systems. In the following, the model is first compared to analytical results for capillary wedge flows for different wedge angles. Comparisons are then made to reduced-g and terrestrial experimental data for both wedge and rectangular groove capillary channels. The example flows selected demonstrate the capability of the model to study systems with fixed or variable control volume V for different cross-sections and different inlet and outlet contact line boundary conditions.

3.1   Analytical comparison

The model is first used to examine viscous-dominated capillary wedge channels flows for which analytical solutions are in hand [6]. The good agreement within

the limit of the viscous analytic solution ($Re < 90$) in fig. 2 and table 2 provides a degree of validation of the *SE* model. Additional computations for greater wedge angles α ($Re > 90$) are performed to identify the limit of the viscous-analytic model and the influence of inertia. The *SE* model captures this presence of increased inertia in the flow and identifies the limits of applicability of the viscous solution. This point is clarified by review of table 2, where quantitative comparisons are made. As expected, deflection differences between the analytic vs. numeric surface predictions increase with Re.
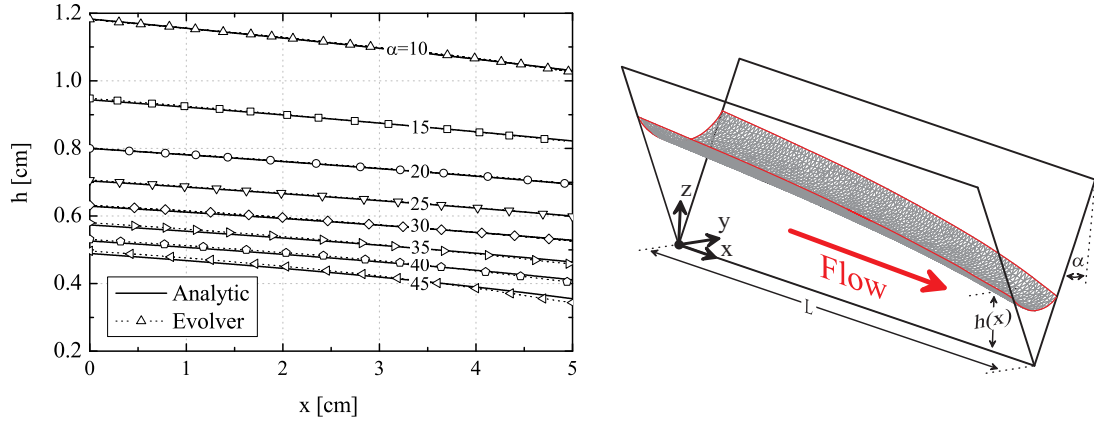

Figure 2: Analytic interface heights for viscous-dominated wedge flows compared to *SE* calculations. The left figure compares the center line of the interfaces for different wedge angles α. The volume $V = 1.160$ ml of the perfectly wetting liquid HFE7500, which is capillary driven with a flow rate of $Q = 0.2$ ml/s. The good agreement validates the *SE* model.

Half-Angle α	10°	15°	20°	25°	30°	35°	40°	45°
Deflection (%)	0.12	0.17	0.18	0.22	0.32	0.77	0.87	1.45
Reynolds number	50	61	71	79	85	93	97	105

Table 2: Deflection values and Reynolds numbers $Re = D_h Q/(A\nu)$ with hydraulic diameter $D_h = 4A/P$, for the comparisons in fig. 2. The deflection increases with increasing Re the presence of inertia is not captured by the viscous-analytic solution.

In this approach the liquid volume V is fixed and independent of gas pressure p_a. Thus, the constant C of eq. (1) has no bearing on the solution. At the inlet and outlet the contact line is free to move with a defined contact angle known from the analytical solution for capillary driven flow.

3.2 Viscous-dominated capillary flows: wedge

In fig. 3 the SE model is compared to experimental data from M. M. Weislogel. Two plots are shown in the figure to demonstrate the accuracy of the method. The first comparison is performed in a reduced gravity environment (parabolic flight) with a constant flow rate of 0.019 ml/s, fig. 3 (lower left). The second comparison plot is selected for a terrestrial experiment and a flow rate of 0.039 ml/s, fig. 3 (lower right). Good agreement is obtained for both environments with errors less than 2% (note the exaggerated scales). Experimental uncertainty of ± 2 px is shown using dashed lines on the figure.
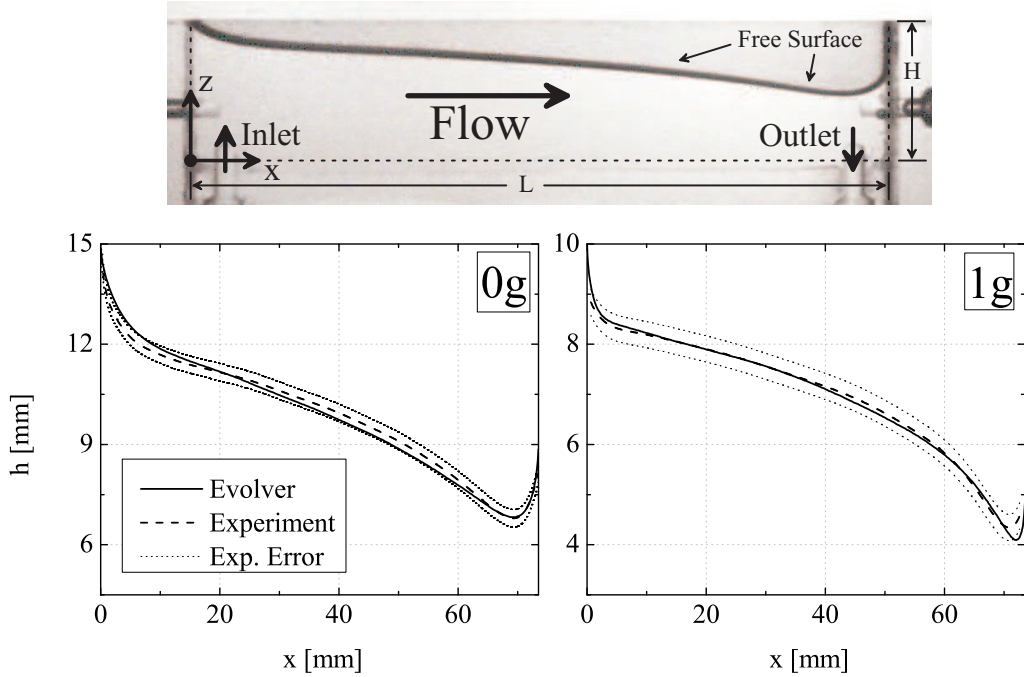

Figure 3: Model comparison with viscous-dominated reduced-gravity (left) and terrestrial (right) capillary flow experiments ($Bo < 1$), where $H = 14.88$ mm, $L = 73.5$ mm, and wedge half-angle $\alpha = 5°$. The test fluid is perfectly wetting Silicone oil with kinematic viscosity $\nu = 10$cs at liquid volume $V = 0.675$ml (left) and $\nu = 5$cs at liquid volume $V = 335$ml (right).

The SE model for the reduced-gravity case is demonstrated in fig. 5. Again, the liquid volume V is fixed and independent of gas pressure p_a. In contrast, the experimental in- and outlet of the test section is at $z = 0$ as shown in fig. 3 (top). The cross-flow is not captured by the SE model, but can be neglected due to high viscous flow ($Re \sim 1$). For this setup mixed pinning and fixed contact angle boundary conditions were applied along the interface boundaries. The additional gravity field for the terrestrial case is implemented with eq. (11).

3.3 Inertia-dominated capillary flows: rectangular groove

The model was also applied to the problem of flow through a rectangular groove-shaped capillary channel as investigated experimentally by Haake et al. [11] using a drop tower. Sample comparisons are presented in fig. 4. The parameters along with a sketch of the flow cross section is shown in fig. 5. As observed from the figure, the interface profiles are in good agreement with the numerical predictions with errors less than 1%. The experiments employ an apparatus that strives to maintain constant pressure at the channel inlet allowing the liquid volume V of the test section to vary. Nevertheless, the constant C of eq. (1) is well-defined by the flow history, which is in turn a function of the flow rate Q. Again, mixed pinning and fixed contact angle boundary conditions at the contact line were applied.
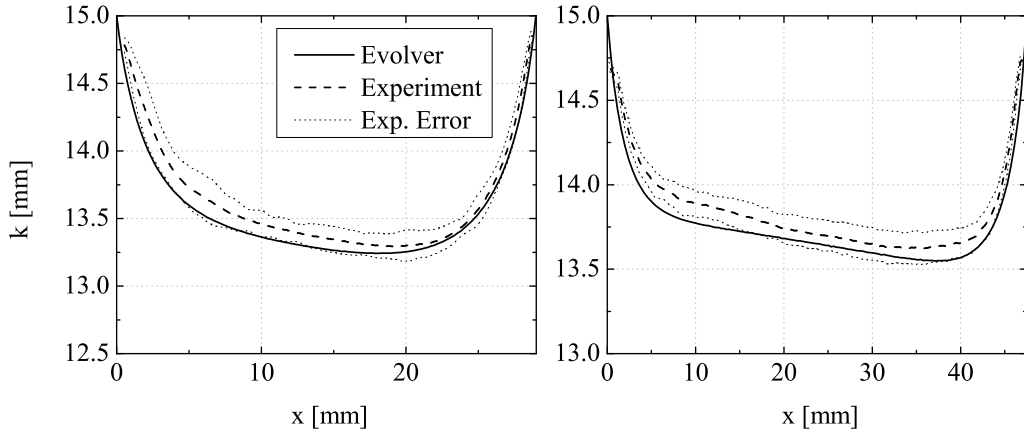

Figure 4: Model comparisons with large capillary length scale zero-gravity drop tower experiments. Flow through open rectangular groove channel, where $a = 5$ mm, $b = 30$ mm, for a perfectly wetting liquid FC-72: (left) length $L = 28.97$ mm and critical flow rate $Q \approx 6.30$ ml/s, (middle) $L = 47.50$ mm and $Q \approx 5.70$ ml/s (note the exaggerated scale).

L	Re	$Q_{crit,num}$	$Q_{crit,exp}$
28.97 mm	1020	6.59 ml/s	6.60 ± 0.10 ml/s
47.50 mm	1004	6.31 ml/s	6.35 ± 0.15 ml/s

Table 3: Reynolds numbers and critical flow rate comparisons for the convective dominated channel flows in fig. 4. The good agreement validates the tool for critical design studies. The code allows flow rate or property changes during the iterations, which is helpful for efficient analysis.

In addition to computing interface profiles and flow rates, the model is found to be capable of computing maximum (or limiting) flow rates for given geometries

and boundary conditions. For example, in similar experiments performed using a parallel plate capillary channel of larger length and inertial scale Rosendahl et al. [8] found that a critical flow limitation in open capillary channels exists that is analogous to choking in compressible duct flows or similar flow limits in open terrestrial channel flows. For such open capillary channel flows, by increasing the flow rate, the liquid pressure decreases causing the free surface to continue to bend inwards. The maximum flow rate is achieved at the instant the free surface no longer balances the pressure difference between the liquid and the surrounding gas. Beyond this point the interface is dynamically unstable, becomes unsteady, and breaks-up causing unsteady gas ingestion into the liquid flow. The SE model of such flows can be used to compute such limits as indicated simply by the solution diverging at the 'critical' flow rate. Sample computational results are provided in table 3 for $Re \sim 1000$ with high accuracy when compared to the results of experiments.
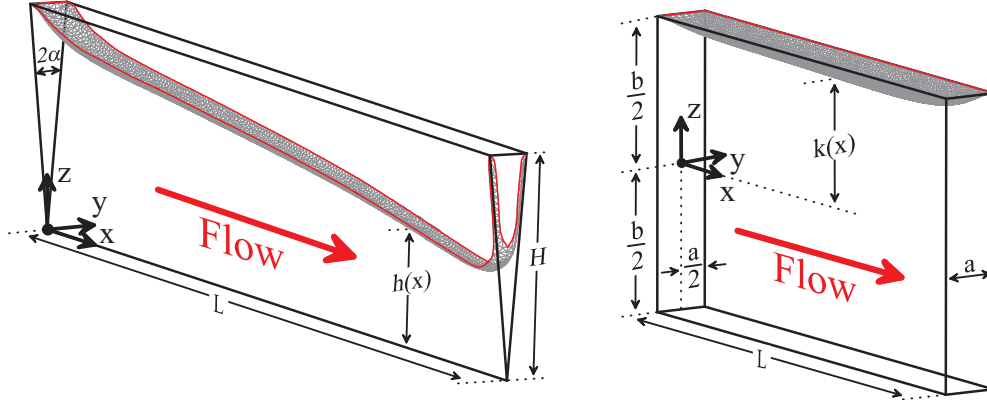

Figure 5: Computed interfaces and parameters for the wedge (left) and the groove (right) experiments. All computations use 10000 grid elements for the interface (~ 1000 elements are shown). With a regular Pentium 4 processor the computational time is approx. 5 min.

4   Summary

In this work an iterative procedure has been implemented to SE to predict steady state flow profiles, flow rates, and flow rate limits along partially open capillary channels. Because of the high computational effort for 3-d numerical Navier-Stokes solvers with interface tracking, the proposed method is attractive as an alternative design tool for parametric studies due to its speed and stability (minutes compared to days). This overview introduces the pressure model and general procedure for capillary wedge flows, but the method is applicable for arbitrary cross-sections inviting further extensions to suit a variety of flow

geometries. The method is benchmarked herein with analytic and experimental data for both viscous- and inertia-dominated flows. Terrestrial and reduced g-environment data is employed, the latter being gathered from parabolic aircraft and drop tower experiments, respectively. The validation of the code for various boundary conditions and channel cross-sections also speaks to the generality of the method. Details of the code are left to the appendix and can be downloaded at http://www.zarm.uni-bremen.de/2forschung/grenzph/publications.

To date, the proposed procedure has been implemented with external subroutines. For standalone operations it is necessary to write the interpolation method directly into the *SE* code.

Acknowledgment

A   Implementation

Missing details for the present implementation are provided here. Again, the present procedure is applied to capillary flow inside a wedge channel (fig. 1). However, it is applicable for other geometries as well.

A.1   Energy equations

The contact line at the interface boundary is either pinned, which can be defined as a fixed constraint, has a defined contact angle θ, which must be included as tension energy, or any combination of both. The contact angle energy can be evaluated from Young's equation and for the wedge channel yields

$$E_{\theta_{in/out}} = -\sigma \cos(\theta_{in/out}) \int_{e_{3/4}} \left(z - \frac{y}{\tan \alpha} \right) dy \tag{9}$$

$$E_{\theta_{wall}} = -\sigma \cos(\theta_{wall}) \int_{e_2} \left(\frac{z}{\cos \alpha} \right) dx, \tag{10}$$

where σ is the surface tension of the liquid. In capillary systems, gravity plays a minor role due to small Bond numbers. Nevertheless, constant accelerations in the z-direction can be implemented as the potential energy $E_g = \rho g \iiint_V z\, dV$, yielding

$$E_g = \rho g \left[\iint_{S_s} \begin{pmatrix} zx \\ 0 \\ 0 \end{pmatrix} \cdot \vec{n}_s\, dS + \frac{L}{2} \int_{e_4} \left(z^2 - \frac{y^2}{\tan^2 \alpha} \right) dy \right]. \tag{11}$$

A.2 Evolver Code

An extract of *SE* is provided here to exemplify the implementation of the energy equations and the iteration scheme for the pressure model. With the definition of the interpolation coefficients,

```
define aa real[6]={inlet_pressure,0,0,0,0,0}
```

the surface integral of eq. (8) can be implemented as an additional quantity,

```
quantity E_p energy method facet_general_integral
scalar_integrand: x4*(aa[0]*x+aa[1]/2*x^2+aa[2]/3*x^3+\
                      aa[3]/4*x^4+aa[4]/5*x^5+aa[5]/6*x^6)
```

The missing edge integral and eqs. (9) and (10) can be defined as constraints for the contact line. To avoid single-letter parameters LL is the parameter for the length L.

```
constraint inlet
formula: x=0
energy:
e1:0
e2:-(z-y/tan(alpha))*sigma*cos(theta_in)
e3:0

constraint outlet
formula: x=LL
energy:
e1:0
e2:(aa[0]*x+aa[1]/2*x^2+aa[2]/3*x^3+aa[3]/4*x^4+aa[4]/5*x^5+\
    aa[5]/6*x^6-sigma*cos(theta_out))*(z-y/tan(alpha))
e3:0

constraint wall
formula: y=z*tan(alpha)
energy:
e1:-z/cos(alpha)*sigma*cos(theta_wall)
e2:0
e3:0
content:
c1:0.5*z^2*tan(alpha)
c2:0
c3:0
```

The additional content is important to correct the liquid volume. To implement the iteration loop described in section 2, it is useful to redefine the iteration command

```
g:::={system "NewPressure.exe"; system "Interpolation.exe";
        read "UpdateCoefficents.txt"; g 5; NewGrid;}
```

With eq. (1), external executables first calculate the pressure at discrete points and later perform the interpolation. The resulting coefficients are stored in the `UpdateCoefficents` textfile which can be read to update the coefficents of the energy quantities `E_p` and the constraint `outlet`. After some iterations, the `NewGrid` function adjusts the finite element grid and stores the new interface location for the next iteration.

References

[1] K. A. Brakke. The Surface Evolver. *Experimental Mathematics*, 1(2):141–165, 1992.

[2] K. A. Brakke. Surface Evolver manual. *Susquehanna University*, 2.26a, 2005.

[3] S. H. Collicott. Example impact of nonuniform acceleration fields on liquids in spacecraft. *J. Spacecraft Rockets*, 44(3):725–727, 2007.

[4] M. A. Walkley, P. H. Gaskell, P. K. Jimack, M. A. Kelmanson, and J. L. Summers. Finite element simulation of three-dimensional free-surface flow problems. *J. Sci. Comput.*, 24(2):147–162, August 2005.

[5] M. Scholle and N. Aksel. An exact solution of visco-capillary flow in an inclined channel. *ZAMP*, 52:749–769, 2001.

[6] M. M. Weislogel and S. Lichter. Capillary flow in an interior corner. *J. Fluid Mech.*, 373:349–378, 1998.

[7] D. E. Jaekle. Propellant management device conceptual design and analysis: Vanes. In *AIAA/SAE/ASME/ASEE 27th Joint Propulsion Conference*, number AIAA 91-2172, pages 1–13, Sacramento, CA, June 1991.

[8] U. Rosendahl, A. Ohlhoff, and M. E. Dreyer. Choked flows in open capillary channels: theory, experiment and computations. *J. Fluid Mech.*, 518:187–214, 2004.

[9] P. S. Ayyaswamy, I. Catton, and D. K. Edwards. Capillary flow in triangular grooves. *J. Appl. Mech.*, pages 332–336, June 1974.

[10] Matlab. Partial differential equation toolbox. The MathWorks Inc., 2005, 7.1.0.246(R16).

[11] D. Haake, U. Rosendahl, A. Ohlhoff, and M. E. Dreyer. Flow rate limitation in open capillary channel flows. *Ann. NY Acad. Sci.*, 1077:443–458, 2006.